# American Journal of Science

## PLAGIOCLASE HOSTED Fe-Ti-OXIDE MICRO-INCLUSIONS IN AN OCEANIC GABBRO-PLAGIOGRANITE ASSOCIATION FROM THE MID ATLANTIC RIDGE AT 13°34' N

OLGA AGEEVA\*,\*\*,†, GERLINDE HABLER\*, DAN TOPA\*\*\*,
THOMAS WAITZ\*\*\*\*, CHEN LI\*, ALEXEY PERTSEV\*\*, THOMAS GRIFFITHS\*,
OLGA ZHILICHEVA\*\*, and RAINER ABART\*

ABSTRACT.    Shape and lattice orientation relations as well as chemical compositions of Fe-Ti-oxide micro-inclusions and plagioclase host crystals in rocks of a gabbro-plagiogranite assemblage from the Mid-Atlantic ridge at 13°34' N were studied using electron back scatter diffraction, transmission electron microscopy and field-emission gun-electron microprobe analyzer. Several evolutionary stages of the micro-inclusion-host assemblages were discerned, starting with precipitation of Fe-Ti-oxides from a super-saturated plagioclase in otherwise unaltered gabbro, followed by transformation and re-crystallization of the micro-inclusions as well as chemical alteration of both inclusions and host during plagiogranite intrusion and subsequent hydrothermal alteration. A detailed sequence of petrogenetic processes could be reconstructed. Fe-Ti-oxide micro-inclusions are the main carriers of the paleo-magnetic record of these rocks, and understanding the transformations affecting Fe-Ti-oxide micro-inclusions in the highly dynamic mid-ocean ridge environment is crucial for interpreting paleo-magnetic data.

Keywords: Fe-Ti-oxide micro-inclusions, magnetite, clouded plagioclase, gabbro, plagiogranite, Mid-Atlantic ridge, crystallographic relations, electron back scatter diffraction

### INTRODUCTION

Rock-forming minerals often contain solid-phase micro-inclusions, whose formation may involve a variety of processes. When subjected to changing conditions such as pressure/stress, temperature, and component activities subsequent to their formation, solid-phase micro-inclusions may transform while embedded in the crystalline matrix of their host. The inherent anisotropy of both inclusion and host crystal are a specific feature of host-inclusion settings. The coupling between external factors and internal crystal structure controls ultimately determines the chemical, microstructural, and textural characteristics of host-inclusion systems. The crystallographic orientation relations, phase assemblage and phase compositions, micro-structures, and textures of inclusion - host systems reflect the character and sequence of events during their genesis and subsequent evolution. Important petrogenetic information may thus be obtained from an analysis of inclusion-host systems.

\* Department of Lithosphere Research, University of Vienna, Althanstrasse 14, 1090 Wien, Austria
\*\* Institute of Geology of Ore Deposits, Petrography, Mineralogy, and Geochemistry (IGEM), Staromonetnyi 35, Moscow, 119017, Russia
\*\*\* Natural History Museum – Wien, Burgerstrasse 7, 10120 Wien, Austria
\*\*\*\* University of Vienna, Faculty of Physics, Physics of Nanostructured Materials, Boltzmanngasse 5, 1090 Vienna, Austria
† Corresponding author: olga.ageeva@univie.ac.at

Needle-shaped, platy and ultra-fine grained dispersed isometric Fe- and Ti- oxide micro-inclusions such as hematite, magnetite, ilmenite and goethite in rock-forming feldspars have been described in numerous papers (Andersen, 1915; Sobolev, 1990; Hargraves and others, 1999; Wenk and others, 2011 and many others). The term "clouded feldspar" refers to feldspars with very fine-grained dispersed inclusions that cause cloudy coloration of feldspar. The term "aventurine feldspar" or "sunstone" is used for feldspars with "aventurization", that is the optical effect caused by reflection of light from oriented plate-shaped inclusions in transparent minerals. Both terms describe the same phenomenon with variations in size, shape, spatial distribution, crystallographic orientation and probably phase composition of micro-inclusions.

Mostly, iron-titanium oxide micro inclusions in feldspar are interpreted as precipitates from exsolution at sub-solidus conditions. The iron which was incorporated into the feldspar crystal structure at high temperatures during magmatic crystallization or high-grade metamorphism is supposed to be exsolved during cooling (Andersen, 1915; MacGregor, 1931; Carstens, 1955; Evans and McElhinny, 1966; Hargraves and Young, 1969; Murthy and others, 1971; McClay, 1974; Armbrustmacher and Banks, 1974; Popov and others, 1978; Davis, 1981; Renne and Onstott, 1988; Sobolev, 1990; Xu and others, 1997; Feinberg and others, 2005; Sengupta and Ray, 2012; Usui, 2013 and others). However, many plagioclases with high iron content remain free of micro-inclusions. This was ascribed to the lack of water, which is believed to play an important role in the development of clouding of feldspar under sub-solidus conditions (Smith, 1974). Alternatively, Fe-Ti-oxide micro-inclusions may also form by simultaneous crystallization with and subsequent overgrowth by plagioclase (Bottinga and others, 1966; Bridgwater and Harry, 1968). Finally, the introduction of Fe ions from an external source during metamorphic (MacGregor, 1931) and metasomatic (Reynolds, 1946; Poldervaart and Gilkey, 1954; Divljan, 1960 and others) overprint and/or during hydrothermal alteration (Trindade and others, 1999, 2001; Diot and others, 2003; Bolle and others, 2003) may be responsible for the formation of iron-titanium oxide micro-inclusions. Three prerequisites are considered crucial for the formation of Fe-Ti-oxide micro-inclusions in plagioclase: Firstly, high-temperature crystallization, re-crystallization or alteration of plagioclase in magmatic or metamorphic systems allow Fe and Ti to be incorporated into the plagioclase lattice in appreciable concentrations. Secondly, subsequent cooling leads to the precipitation of Fe-Ti-oxide phases within plagioclase. Thirdly, water is needed to catalyze precipitation. Dehydration of nearby hydrous minerals (Touret, ms, 1969) or water incorporated in plagioclase during its crystallization (Smith, 1974) may serve as catalyzing agents.

Iron-titanium oxide micro-inclusions are excellent recorders of the paleomagnetic field (Evans and McElhinny, 1966, Hargraves and Young, 1969, Murthy and others, 1971; Davis, 1981; Morgan and Smith, 1981; Renne and Onstott, 1988; Xu and others, 1997; Selkin and others, 2000; Renne and others, 2002). Due to their single-domain structure and due to protection from the rock matrix by the host mineral, Fe-Ti-oxide micro-inclusions are considered as reliable paleomagnetic monitors (Hargraves and Young, 1969; Xu and others, 1997; Feinberg and others, 2005). In this context, it is important to distinguish between primary and secondary Fe-Ti-oxide micro-inclusions. Remanent magnetization may have been attained during primary magmatic or metamorphic crystallization or during subsequent re-crystallization and/or hydrothermal alteration. Xu and others (1997) have shown that size and phase composition of Fe-Ti-oxide micro-inclusions from Archean mafic rocks determine their paleomagnetic information content. Other studies report on the role of primary and secondary iron oxide micro-inclusions in hydrothermally altered granitoids (Trindade and others, 1999, 2001; Nakamura and Nagahama, 2001; Diot and others, 2003;

Bolle and others, 2003) and in oceanic gabbro (Usui, 2013). Extraction of absolute geomagnetic paleointensity from single plagioclase crystals was developed in the early 2000s. By this method artifacts caused by alteration of samples during the commonly used Thellier–Thellier analyses can be avoided (Cottrell and Tarduno, 1999; Smirnov and others, 2003; Tarduno and others, 2006).

Furthermore, phase relations in the Fe-Ti-oxides system are highly sensitive to redox state (Sauerzapf and others, 2008; Degi and others, 2009). This is why phase content combined with chemical compositions and microstructures may be used to infer the evolution of redox state during primary crystallization and subsequent evolution of Fe-Ti-oxide micro-inclusions.

Determination of the nature and chemical compositions of Fe-Ti-oxide micro-inclusions may be difficult due to small size. In many early works magnetite, hematite, ilmenite and goethite micro-inclusions were described based on light-optical microscopy. Modern studies employing electron microscopy often reveal more diverse phase assemblages and chemical compositions than reported earlier (Anderson, 1966; Kraeft and Saalfeld, 1967; Xu and others, 1997; Feinberg and others, 2005; Wenk and others, 2011).

Morphology and shape orientation of Fe-Ti-oxide micro-inclusions in rock-forming plagioclase have been discussed in many studies. Several nanometers to hundreds of micrometers sized dust-like, needle-, plate-shaped or isometric inclusions have been described based on optical methods including universal stage measurements. The shape orientations of micro-inclusions were found to follow rational directions of the plagioclase-host. Two groups of regularities have been found. A first group comprises elongated inclusions lying on cleavage planes, twin boundaries or other major crystallographic planes and directions of plagioclase, such as (010), (100), (001), [100], [$\bar{1}$01], [1$\bar{1}$0], and the rhombic section (Reynolds, 1936; Philpotts, 1966; Bridgewater and Harry, 1968; Armbrustmacher and Blanks, 1974; Fleet, 1982; Usui and others, 2006). A second group is represented by plate-shaped inclusions generally oriented parallel to low indexed plagioclase lattice planes such as (112), (1$\bar{1}$2), (150), (1$\bar{5}$0) and some others, whereas needle-shaped inclusions are oriented perpendicular to these planes (Andersen, 1915; Divljan, 1960; Kraeft and Saalfeld, 1967; Popov, and others, 1978; Sobolev, 1990).

Comparatively little information is available on the crystallographic orientation relations between plagioclase host and Fe-Ti oxide micro-inclusions. Wenk and others (2011) identified specific crystallographic orientation relations between magnetite and ilmenite inclusions and plagioclase host in anorthositic gneiss with magnetite [110] and ilmenite [100] parallel to plagioclase [001], magnetite (111) sub-parallel to plagioclase (120), and ilmenite (001) sub-parallel to plagioclase ($\bar{1}$20). Needles are elongated parallel to [110] for cubic magnetite and parallel to [100] for rhombohedral ilmenite, and the needle orientation direction is consistently parallel to [001] of plagioclase. Wenk and others (2011) concluded that close packed oxygen atoms determined the orientation of the exsolved magnetite, and channels formed by silica and alumina tetrahedra in plagioclase host restricted the morphology of magnetite to needles.

In this communication we investigate Fe-Ti-oxide micro-inclusions in plagioclase crystals from plagiogranites and gabbros dredged from the Mid Atlantic Ridge at 13°34' N. We present both shape- and crystallographic orientation relations between the Fe-Ti-oxide micro-inclusions and the plagioclase host crystals, and study their chemical and textural evolution during successive stages of gabbroic and plagiogranite magmatism, as well as hydrothermal alteration. The systematics of alteration phenomena are then used to reconstruct the petrogenetic processes that were active in the dynamic environment of the young oceanic crust. In this context, analyzing mineral micro-inclusions is particularly useful, because the inclusions are embedded in a

structurally and chemically well-defined environment and thus are sensitive monitors for alteration processes.

<div align="center">METHODS</div>

<div align="center">*Sampling*</div>

Samples were selected from the material collected during sea floor dredging on the gabbro–peridotite massif at 13°28′–13°35′ N Mid-Atlantic ridge (MAR). During expeditions of R/V Professor Logachev in 2007 to 2011 besides gabbro and peridotite oceanic plagiogranites (OPG), amphibolites and a series of hydrothermal sulfide fields were discovered in the massif. The OPGs associated with amphibolite and gabbro were dredged at 8 stations of the studied region (Pertsev and others, 2012).

Fe-Ti oxide micro-inclusions were observed in two types of rocks: (1) gabbro intruded by oceanic plagiogranites, which is referred to here as "modified gabbro"; (2) gabbro without obvious plagiogranite influence, which is referred to here as "non-modified gabbro". Both types of rocks were sampled at the same dredging station.

<div align="center">*Universal Stage Measurements*</div>

A universal stage was used for determining shape orientations of about 50 needle- and plate- shaped micro-inclusions previously studied with EBSD (Electron backscatter diffraction). The shape orientations of Fe-Ti-oxide needles or plates were determined and plotted in stereographic projection together with selected crystallographic directions of the plagioclase host. Then these data were combined with crystallographic orientation data previously determined with EBSD. Through this the full relations between shape- and crystallographic orientation of the inclusion-host system could be determined. The reproducibility of universal stage measurement depended on size and inclination of the needle or plate with respect to the thin section surface and varied from 2° to 7°.

<div align="center">*Cathodoluminescence (CL)*</div>

CL investigations were done on the electron-probe micro-analyzer "Cameca MS-46" at the IGEM RAS (Moscow). The instrument is equipped with a Videoscan 285 digital high-resolution camera with software Viewer. The parameters for obtaining high-quality CL images were a scan area of 300x300 μm, a gain of 100, an exposure time of 240 s, a probe current of 15 nA, and an accelerating voltage of 20 kV.

<div align="center">*Electron Probe Microanalysis (EPMA)*</div>

Electron probe microanalyses were performed with a JEOL Hyperprobe JXA 8530F instrument, at the Naturhistorisches Museum Wien (Austria). The instrument is equipped with a field emission electron gun, five wavelength dispersive spectrometers (WDS) and an energy dispersive spectrometer (EDS). Settings were at an accelerating voltage of 15 kV, a beam current of 20 nA, counting times of 10 seconds for peaks and 5 seconds for backgrounds. Point analyses along the two profiles were done with focused beam (estimated beam diameter 0.07 μm), otherwise a defocused beam was used (beam diameter 2 μm). The standards and lines used for plagioclase analyses are: olivine for Si$K\alpha$, Fe$K\alpha$ and Mg$K\alpha$, pure oxides for Al$K\alpha$ and Ti$K\alpha$, wollastonite for Ca$K\alpha$, tephroite for Mn$K\alpha$, synthetic NaCl and KCl for Na$K\alpha$ and K$K\alpha$, respectively. Detection limits (in ppm) for measured elements in the plagioclase matrix under these conditions are: Ti, Mn, Fe: ~100, Si, Al: ~70, Ca, K, Na and Mg: 50. X-ray element distribution maps (stage movements for 450x350 pixels, with step size of x = 0.1 and y = 0.1 μm, for an area of ~45x35 μm$^2$) were acquired at an acceleration voltage of 15 kV, a beam current of 20 nA, a beam diameter of 0.07 ìm and a dwell time of 200 ms/pixel. Silica, Ti, Ca, Fe and Na were measured in the first run followed by Al, K, Mn and Mg in the second run, using WDS.

*Electron Back Scatter Diffraction (EBSD)*

Electron Backscatter Diffraction (EBSD) analyses of a mechanically and chemo-mechanically polished thin section were carried out using a FEI Quanta 3D FEG instrument at the Laboratory for Scanning Electron Microscopy and Focused Ion Beam Applications at the Faculty of Geosciences, Geography and Astronomy at the University of Vienna (Austria). The instrument is equipped with a Schottky field emission electron gun and an EDAX Pegasus Apex IV detector system consisting of an EDAX Digiview IV EBSD camera as well as an Apollo XV Silicon Drift Detector for Energy dispersive X-ray spectrometry. The EDAX OIM DC v6.2.0 version has been used for single point EBSD analysis and for orientation mapping in combination with qualitative EDX analysis. A total of 322 single point data were collected in 4 different sample domains, comprising 117 magnetite inclusions, 99 ilmenite inclusions and 106 analyses of plagioclase host adjacent to the inclusions. Electron beam settings were at 15kV accelerating voltage, about 4 nA beam current in analytic mode at a working distance of 14 mm and at 70° sample tilt. For single point analyses a 2x2 binning (431x431 pixels pattern size) and averaging over 5 pattern frames has been used to reduce noise in the EBSPs, whereas for mappings, a 4x4 binning (215x215 pixels pattern size) was used to collect orientation data from single frame pattern. Plagioclase was indexed as triclinic phase (Laue Group -1, a=8.155 Å, b=12.821 Å, c=7.14 Å; $\alpha$=93.965°, $\beta$=116.4°, $\gamma$=89.46°), magnetite as cubic phase (Laue Group m3m, a=8.396 Å) and ilmenite as di-trigonal phase (Laue group -3m; a=5.123 Å, c=13.76 Å). Using the lower trigonal symmetry -3 for ilmenite would yield two orientation solutions (pseudosymmetry), which are not distinguishable by EBSD. Therefore a higher symmetry with additional mirror plane was used. Hough parameters for orientation maps were at a binned pattern size of 160 pixels, a Theta step size of 1°, and a Rho-fraction of 78 percent. The classic low resolution Hough type with a 9x9 convolution mask has been applied for indexing a minimum of 3 and a maximum of 15 peaks at a minimum peak distance of 10 pixels. The interplanar tolerance angle was at 2°. For single point orientation data Hough settings (binned pattern size, Rho fraction, convolution mask) and the maximum number of peaks were adjusted for each analysis point in order to reach a distinct, statistically reliable orientation solution.

Due to the significantly different scattering behavior of plagioclase compared with magnetite and ilmenite the camera settings and pattern processing (for example camera exposure, gain and histogram normalization filter) were adjusted to avoid oversaturation of ilmenite and magnetite patterns. Therefore, the contrast of plagioclase EBSPs was very low, resulting in a low image quality parameter and a low indexing rate for Pl analyses especially for small step sizes below 100 nm. Whereas ilmenite and magnetite during mapping were entirely indexed without data processing or cleaning, the rate of indexed plagioclase analyses is strongly dependent on the map step size. Indexed raw data yielded 4 to 56 percent indexed points for step size 80 nm, 15 to 55 percent indexed points for step size 100 nm and 59 percent and 70 percent indexed points for maps with 110 nm and 130 nm step sizes, respectively. Cleaning by Grain CI standardization (unifying the CI-value of neighboring points with the same orientation) and a Neighbor Orientation Correlation cleaning procedure level 2 (changing orientation of an analysis point according to the neighbor orientation, if 4 neighboring points in hexagonal grid have the same orientation) led to a significant increase in the fraction of indexed plagioclase analyses. After cleanup the number of indexed grains increased up to 95 percent for maps with step size 80 nm, to 70 to 99 percent for step size 100 nm and to 94 and 98 percent for maps with step size 110 nm and 130 nm respectively.
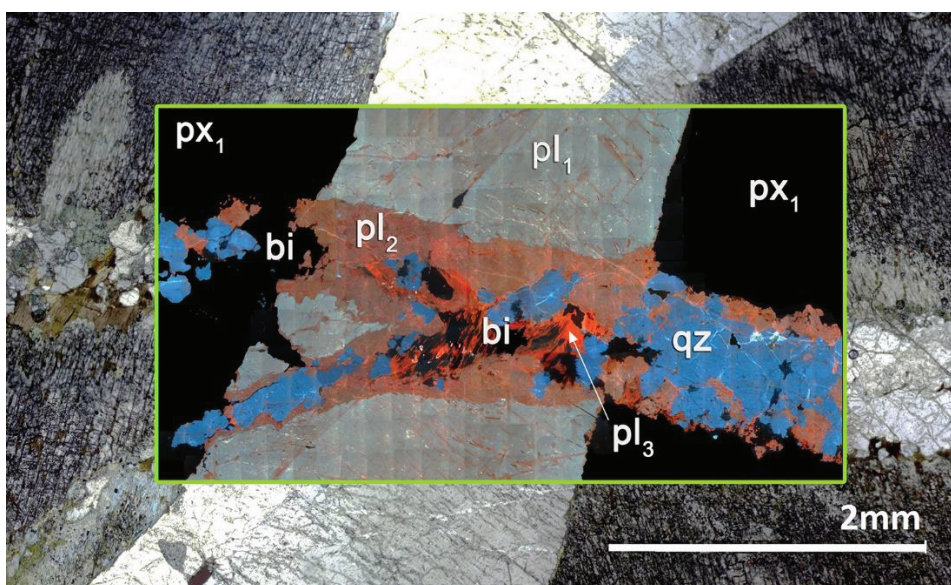
Fig. 1. Optical and cathodoluminescence (insert in green frame) images show an OPG vein within "modified gabbro": $pl_1$ – early-magmatic (gabbroic) plagioclase; $pl_2$ – OPG plagioclase; $pl_3$ – hydrothermal plagioclase; bi – biotite; qz – quartz; px – pyroxene.

### Transmission Electron Microscopy (TEM)

A site and orientation specific TEM foil was prepared by focused ion beam (FIB) preparation using a FEI Quanta 3D FEG instrument at the laboratory for scanning electron microscopy and focused ion beam applications at the Faculty of Geosciences, Geography and Astronomy at the University of Vienna (Austria). The foil was prepared from a plagioclase grain enclosing numerous oxide needles with parallel orientation at a small angle with respect to the sample surface. The foil was oriented approximately perpendicular to the oxide needles long axes. The foil was extracted and transferred by *in situ* lift-out to an Omniprobe™ Cu grid. Final foil thinning to 90 nm thickness was applied to a 20 × 10 micrometers sized area. During the different sputtering steps successively lower Ga ion beam currents down to 30 pA were applied at an accelerating voltage of 30kV in order to minimize amorphization and redeposition. A Philips CM 200 TEM equipped with a double-tilt holder was used to obtain TEM bright field images and selected area diffraction pattern for studying the orientation relationship between the precipitate and the surrounding crystal. To avoid knock-on damage by the electron beam the acceleration voltage was set to a rather low value of 80 kV.

### RESULTS

### Mineralogy of Studied Samples

"Non-modified gabbro" consists of sub-idiomorphic 0.3 to 0.7 centimeter sized grains of magmatic plagioclase, orthopyroxene and clinopyroxene, where the latter often has amphibole rims. The coarse grained plagioclase is mostly untwinned. In some grains Carlsbad twins were observed. The coarse grained plagioclase is un-twinned. Fine grained interstitial plagioclase with polysynthetic albite twins indicates plastic deformation. In addition xenomorphic up to 0.3 centimeter sized grains of Fe-Ti-oxides and fine grains of accessory apatite accumulating between grains of rock-forming minerals occur.

In "modified gabbro" three mineral assemblages can be discerned. An early magmatic assemblage of 0.5 to 1 centimeter sized gabbroic minerals comprising plagioclase + clinopyroxene + orthopyroxene is cut by OPG in the form of up to 0.7 centimeter wide biotite + quartz + plagioclase veins containing subordinate hornblende, zircon, titanite, apatite, fine grained isometric clinopyroxene and Fe-Ti-oxide grains. The third assemblage is represented by late quartz and albite locally with xenomorphic clinopyroxene. Actinolite and chlorite pertain to hydrothermal mineralization, which is mainly observed in areas of OPG mineralization. The OPG veins have sharp contacts to the host gabbro (fig. 1); in some areas coarse-grained minerals of the gabbro assemblage are resorbed by aggregates of OPG mineralization with formation of magmatic breccias. Accessory titanite and zircon are located in the OPG breccias and veins and are precipitated in areas affected by hydrothermal alteration.

*Fe-Ti-oxide Micro-inclusions in Plagioclase*

In "non-modified gabbro" only coarse grained plagioclase is clouded by abundant, very fine grained Fe-Ti-oxide micro-inclusions. No micro-inclusions are observed in interstitial fine-grained plagioclase. In "modified gabbro" different generations of plagioclase are discerned, where the successive plagioclase generations show different Fe-Ti-oxide micro-inclusion abundances and characteristics. In the following the features of the micro-inclusions in both the "non-modified gabbro" and the "modified gabbros" are described in connection with the hosting plagioclase- and host-rock characteristics.

In "non-modified gabbro" the coarse grained plagioclase host abundant dust-like micro-inclusions and very thin needles, 0.02-0.1 microns wide and several tens of micrometers long. The needles form groups with different well-defined shape preferred orientations (fig. 2A). These micro-inclusions are most abundant in the core regions of the feldspar grains and absent in the peripheral regions and adjacent to cracks.

As compared to plagioclase from "non-modified gabbro", plagioclase from "modified gabbro" contains larger Fe-Ti-oxide micro-inclusions, which exhibit less strong shape preferred orientation (fig. 2B). The micro-inclusions vary from 0.05 up to 40 micrometers in width and from 0.5 to 100 micrometers in length (figs. 2 B-L). They occur as needles and ossicles (figs. 2B, 2D, 2E, 2H, 2K and 2L), idiomorphic (fig. 2F), oviform (fig. 2G) and irregularly shaped, rounded plates (figs. 2I-J); discontinuous (figs. 2B, 2C, 2G, 2H, 2J and 2L); homogeneous ilmenite micro-inclusions (fig. 2G) and magnetite-ilmenite intergrowths, where oriented ilmenite lamellae are hosted in magnetite needles or plates (figs. 2C-2F and 2I-2K). It should be noted that highly abundant Fe-Ti oxide micro-inclusions are typical for relict (gabbroic) plagioclase and are restricted to areas that only experienced minor modification and recrystallization. Plagioclase from the OPG contains only few plates and needles of homogeneous ilmenite, and hydrothermal plagioclase is usually free of micro-inclusions. In relic gabbroic plagioclase, domains free of micro-inclusions occur adjacent to large plates of ilmenite-magnetite inclusions (fig. 2C). An abrupt change in the quantity of Fe-Ti-oxide micro-inclusions is observed in gabbroic plagioclase at the boundary with OPG- or hydrothermal plagioclase (fig. 2G). Micro-inclusions in these areas are usually resorbed and discontinuous needles are common (figs. 2G and 2H).

Extremely fine Fe-Ti-oxide needles occurring as inclusions in plagioclase from "non-modified gabbro" were studied using TEM and universal stage light microscopy. Fe-Ti-oxide micro-inclusions hosted in plagioclase of "modified gabbro" were sufficiently large to be studied by EBSD. About 200 of these micro-inclusions were analyzed by single-point EBSD measurements.
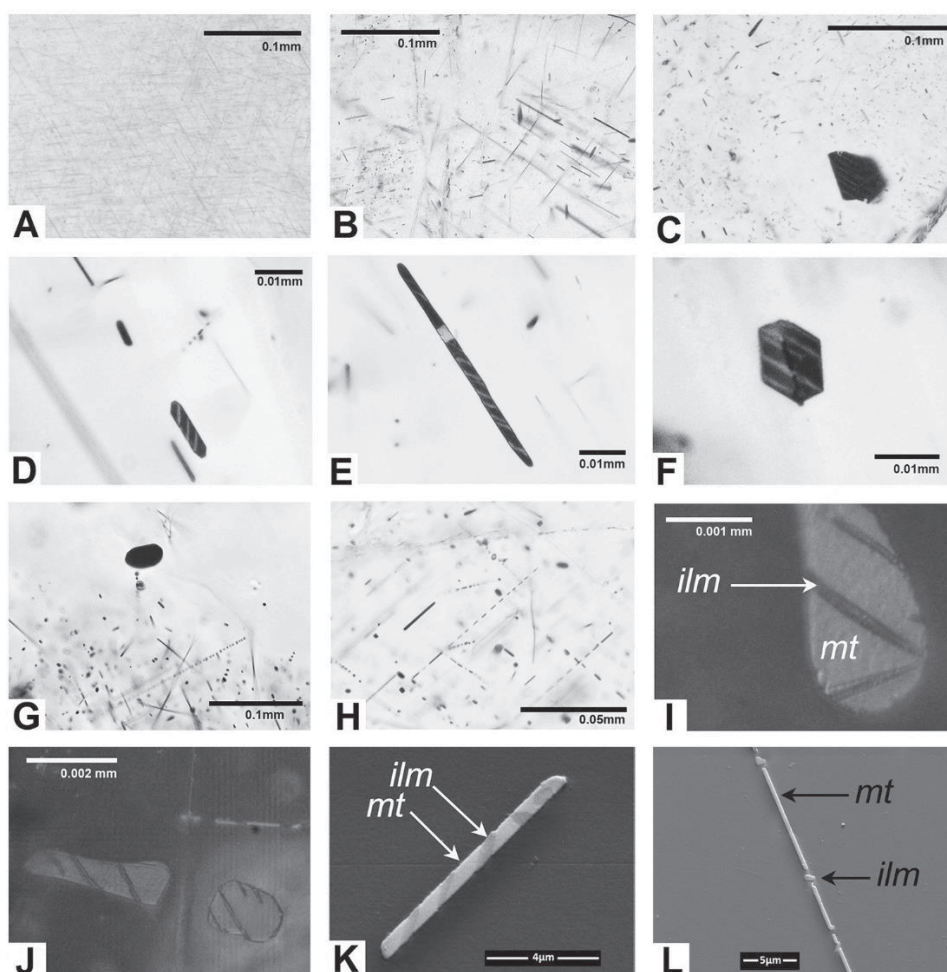
Fig. 2.  Images showing morphology and phase composition of Fe-Ti-oxide micro-inclusions in plagioclase of OPG-intruded gabbro: optical images in transmitted (A-H) and reflected (I-J) light, and secondary electron images (K-L); micro-inclusions from "non-modified gabbro" (A) and "modified gabbro" (B-L) are represented by thin magnetite needles (A), ilmenite plates (G), magnetite-ilmenite needles, ossicles and plates (B-F, L-H).

### *Crystallographic Orientation Relations in "Non-modified Gabbro"*

Micro-inclusions in plagioclase of "non-modified gabbro" display a strong shape preferred orientation. Needle long axes are preferably oriented in several directions, which are mainly orthogonal.

The most abundant group of magnetite needles was studied by transmission electron microscopy (TEM). The crystallographic orientation relationship with the surrounding plagioclase crystal was determined by selected area electron diffraction (SAED). The TEM bright field image in figure 3A shows the ellipse shaped cross section of a magnetite needle (dark contrast) with a diameter of less than 300 nm. Figures 3B and 3C are SAED patterns from the micro-inclusion and the surrounding plagioclase host, respectively, showing that the magnetite [112] zone axis is parallel to
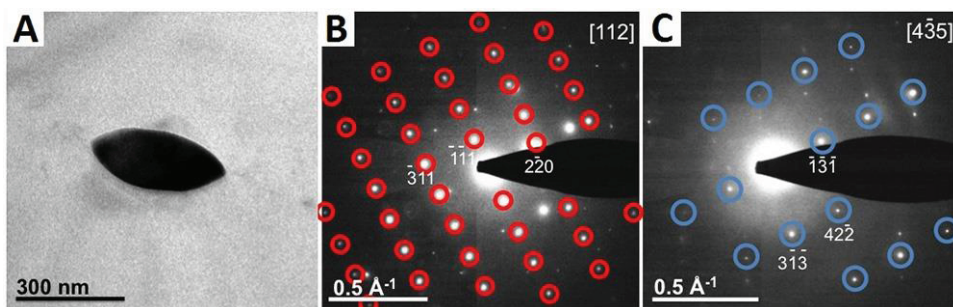
Fig. 3. (A) TEM bright field image showing ellipse-shaped cross section of a magnetite needle; (B) and (C) are SAED patterns from the magnetite needle and the surrounding plagioclase matrix, respectively.

the $[4\bar{3}5]$ zone axis of the surrounding plagioclase. Furthermore, the $(2\bar{2}0)$ planes in magnetite are parallel to the (131) planes of plagioclase.

### Crystallographic Orientation Relations in "Modified Gabbro"

Fe-Ti-oxide micro-inclusions were studied in relic and weakly modified domains in several differently oriented plagioclase crystals. The results from the plagioclase grain with the largest number of inclusions studied are shown in figure 4. For other plagioclase crystals the same orientation relations were found.

The studied plagioclase is twinned after the Carlsbad and albite twin laws (fig. 4A). Albite twins can be identified as deformation twins as they are commonly tapered, terminate within plagioclase grains and are inhomogeneously distributed within grains. Carlsbad twinning divides the crystal into two large domains ("Right" and "Left" twins in fig. 5A) elongated along the (010) twin plane. Both Carlsbad twins are in turn twinned after the albite twin law with the same (010) twin plane. The dominant albite twin orientation studied in one of the two Carlsbad twins is referred to as "Right-I" twin. The corresponding albite twin is referred to as "Right-II" twin. The two related crystal orientations in the other Carlsbad twin are referred to as "Left-I" and "Left-II" twins. The poles of some major crystallographic planes are shown in stereographic projection in figure 4A. This nomenclature does not reflect any sequence of twin formation, it is merely used in a descriptive sense. The largest amount of orientation data is available from "Right-I" orientation (fig. 4B).

*Orientation of magnetite relative to «Right-I» plagioclase.*—Several types of orientation relations between magnetite micro-inclusions and host plagioclase were found in the "Right-I" domains. The most abundant inclusion (type "1" in table 1, red dots in black circles in fig. 4B) have $\{111\}mt$ oriented parallel to $(112)PL$ and two of the $(110)mt$ planes parallel to $(1\bar{5}0)PL$ and $(131)PL$. These inclusions show a pronounced shape orientation with needles elongated parallel to $[111]mt$ perpendicular to $(112)PL$. A group of inclusions related to this type, "$1_{rot}$", is characterized by rotation of magnetite around the pole of $(111)mt$ which is parallel to $(112)PL$ (fig. 4B, red dots). In another abundant orientation relation $(110)mt$ is parallel to $[1\bar{1}0]PL$ (fig. 4B, on the right). The shape orientation is often the same as in type "1", but some needles are elongated along their $[110]mt$ direction, which lies in the $(112)PL$ plane.

Another group of orientations, referred to as type "2" in table 1 and in figure 4B (green dots in black circles) is represented by abundant inclusions with $(111)mt$ parallel to $(1\bar{5}0)PL$ and one of the $[110]mt$ parallel to $[001]PL$, which is also the direction along which most of the needles are elongated. A group of orientations, related to this type (group "$2_{rot}$"), is characterized by free rotation of magnetite around
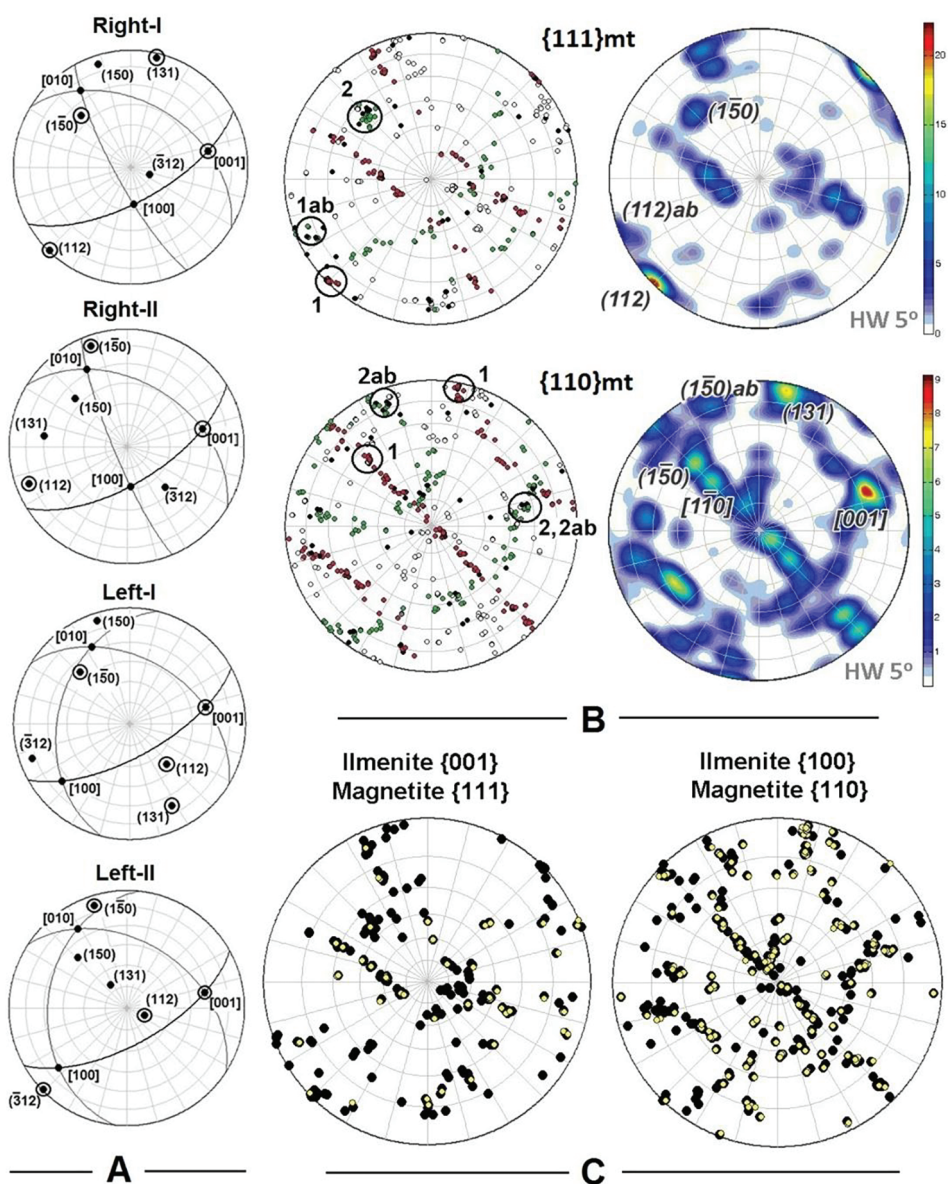
Fig. 4. Crystallographic orientation relations between micro-inclusions and plagioclase host as obtained from EBSD analysis (based on the study of 69 magnetite micro-inclusions). (A) Pole figures (equal angle, upper hemisphere) showing crystallographic orientations of twins in the studied plagioclase grain. Double circles indicate the most important crystallographic elements related to the magnetite orientation in different types of twins. (B) On the left: the pole figures of crystallographic orientations of magnetite {111} and {110}. Red and green dots indicate magnetite orientations corresponding to types "1", "2" (in black circles), "$1_{rot}$" and "$2_{rot}$" in "Right-I" twin. Black dots indicate orientations of magnetite of "$1_{ab}$" and "$2_{ab}$" (in black circles) orientation types in "Right-II" twin. White dots indicate magnetite attributed to "Left-I" and "Left-II" twins. On the right: the ODF (Orientation Distribution Function) plots for the neighboring pole figures (and scales of multiples of the uniform distribution). The plagioclase crystallographic elements of "Right-I" and "Right-II" plagioclase twins according to their position on stereographic plots (A) are added to the magnetite ODF plot. (C) Crystallographic relations between magnetite and ilmenite in ilm-mag intergrowths: black dots indicate magnetite orientation, the yellow ones indicate ilmenite orientation.
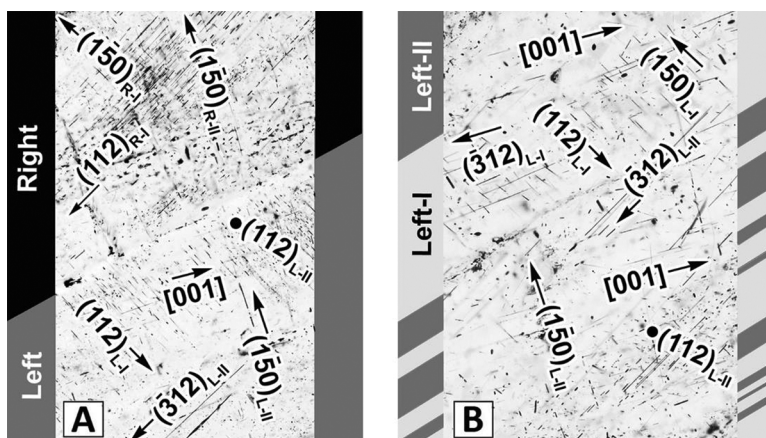
Fig. 5. Change of micro-inclusion shape orientation at the border between two Carlsbad (A) and albite (B) twins; labels and arrows indicate magnetite needles oriented parallel to the poles of planes of plagioclase twins "Right-I", "Right-II", "Left-I" and "Left-II" (R-I, R-II, L-I and L-II respectively); parallel orientation of needles oriented parallel to plagioclase poles Pl(112) of the "Right-I" and Pl(-312) of the "Left-II" can be observed, similarly needles are oriented parallel to the Pl(1-50) in "Right-II" and "Left-II" twins; needles oriented parallel to the Pl($\bar{1}$12) of pole of the "Left-II" twin are sub-perpendicular to the sample surface and therefore are seen in projection (indicated by black circles). The orientation of the image corresponds to orientations of EBSD plots in figures 4 and 6.

the common pole of $(1\bar{5}0)PL$ (fig. 4B, green dots). In this case the needles are elongated in their $[111]mt$ direction, which is aligned perpendicular to $(1\bar{5}0)PL$ or, in some cases, in their $[110]mt$ lying in the $(1\bar{5}0)PL$ plane.

Orientation relations pertaining to the above mentioned types occur in more than 80 percent of the studied inclusions in relict (gabbroic) plagioclase of the "modified gabbro". For the majority of the remaining magnetite micro-inclusions different crystallographic orientation relations with the plagioclase host were found (table 1). Some magnetite grains have their crystallographic orientations aligned with major crystallographic planes and directions of the plagioclase, such as $(001)PL$, $(010)PL$ *et cetera* (table 1). In some cases, the inclusions of this group have their needle long axis lying within plagioclase twin planes.

*Magnetite micro-inclusions and plagioclase twinning.*—The studied plagioclase is twinned after the Carlsbad and albite twin laws. It should be noted that some crystallographic elements have the same or close orientation in these types of twins (fig. 4A). This is why some micro-inclusions have the same orientation in different plagioclase twin systems. For example, many inclusions are elongated and regularly oriented parallel to the $[001]PL$ direction, which is the same direction for both Carlsbad and albite twins.

Albite twinning leads to different kinds of regularities. Usually the micro-inclusions show good lattice correspondence with the plagioclase host only in the dominant albite twin domain (here "Right-I"). The subordinate twin orientation (here "Right-II") has inclusions showing less strong crystallographic orientation relations (black dots in the fig. 4B). Often one of the directions is parallel or sub-parallel to the (150)- and (1$\bar{1}$2)- planes which are close to parallel to ($1\bar{5}0$) and (112) of the related twin orientation. Other micro-inclusions show orientations ("$1_{ab}$" and "$2_{ab}$" in fig. 4B) that are similar to the main types distinguished for "Right-I" twin, that is $\{111\}mt$ parallel to plagioclase (112) or ($1\bar{5}0$).

Needle orientations change abruptly at the boundaries between "Right" and "Left" Carlsbad twins (fig. 5A). This is in line with the fact that the $(112)PL$ planes to

Table 1

*Crystallographic orientation relations between magnetite micro-inclusions and plagioclase obtained from EBSD measurements*

| Orienta-tion Type | Mt(111) // Pl(hkl): | Mt(110) // Pl(hkl) or Pl[uvw]: | Mt(100) // Pl(hkl) or Pl[uvw]: | Mt(111) // Pl(hkl) or Pl[uvw]: | Mt(110) // Pl(hkl) or Pl[uvw]: | Mt(100) // Pl(hkl) or Pl[uvw]: |
|---|---|---|---|---|---|---|
| 1 * | **(112)** | $(1\bar{5}0)$; ~(131) | | [010] | $[1\bar{1}0]$ | |
| $1_{rot}$ * | **(112)** | $[1\bar{1}0]$ | | [110] | | |
| $1_{rot}$ * | **(112)** | (150) | | [101] | | |
| $1_{rot}$ * | **(112)** | | | [100] | $(04\bar{1})$ | |
| 2 * | $(1\bar{5}0)$ | **[001]** | | $[\bar{1}01]$ | [001] | |
| $2_{rot}$ * | $(1\bar{5}0)$; (112) | | | (021) | [100]; $[1\bar{1}0]$ | |
| $2_{rot}$ * | $(1\bar{5}0)$ | | (021) | [310] | | |
| $2_{rot}$ * | $(1\bar{5}0)$ | | | | [100] | [010] |
| * | (150) | [001] | | | [001] | |
| * | (150) | | | | (010) | |
| | (150) | ~ (021) | | | $[1\bar{1}0]$ | |
| | (150) | | | | $(0\bar{2}1)$ | |
| ≠3 * | **$(\bar{3}12)$** | ~ (112) | $(0\bar{2}1)$ | | (120) | |
| | $(\bar{3}12)$ | $[1\bar{1}2]$ | | | $(1\bar{5}0)$ | |
| | $(\bar{3}12)$ | | ~ $[1\bar{1}0]$ | | $(1\bar{1}2)$ | |
| | (001) | [110] | | | | [112] |
| | ~ (001) | [001] | | | | (100) |
| | (001) | | | | | [100] |
| | (101) | ~ (010) | | | | [001] |
| | [100] | (001) | | | | $(04\bar{1})$ |

Notice. (*) - orientation relations found in more than one micro-inclusion. The data are shown for all types of twins; types "1", "2", "$1_{rot}$" and "$2_{rot}$", - orientation in the most intensely studied micro-inclusions in "Right-I"; type "3" - orientation identified for magnetite micro-inclusions in "Left" twins. Bold font shows the most abundant direction of needle elongation.

which the majority of the micro-inclusions is perpendicular, have different orientation in two related Carlsbad twins (fig. 4A). Nevertheless, some inclusions have the same orientation as the majority of inclusions in the neighboring Carlsbad twin due to: (i) parallel orientation of $(1\bar{5}0)PL$ in Carlsbad twins (fig. 4A), parallel orientation of $(1\bar{5}0)PL$ and $(150)PL$ in albite twins, and due to the same orientation of [001]PL in both Carlsbad- and albite twins. Moreover, some magnetite needles in "Left-II" twin are elongated perpendicular to (-312)PL. This plagioclase crystallographic plane is parallel to (112)PL of the "Right-I" twin (figs. 4A and 5). The same correspondence exists between "Right-II" and "Left-I" twins (figs. 4 and 5).

The magnetite needles and plates in many cases cross two or more twin boundaries (predominantly albite twins). For many inclusions the crossing of twin boundaries does not result in essential change of the micro-inclusion orientation. This is expectable for magnetite needles crossing the boundaries in directions that correspond to parallel directions in both plagioclase twins, that is $(1\bar{5}0)PL$ and $(150)PL$ in albite twins
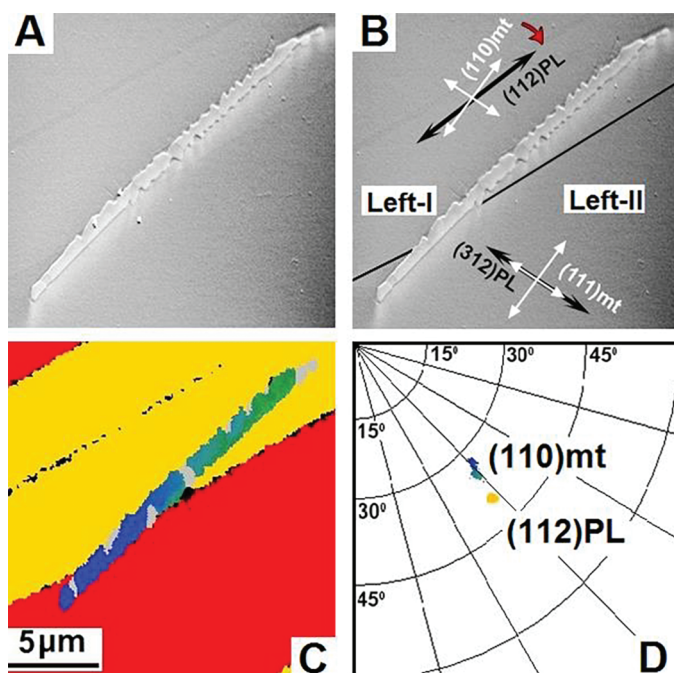
Fig. 6. Change of shape- and crystallographic orientation of a micro-inclusion extending across an albite twin boundary. The part of the needle located in the "Left-I" twin individual is corroded and its Mt(110) plane "rotates" towards PL(112) of the enclosing twin individual ("Left-I"). (A) SEM image. (B) SEM image with schematic indication of crystallographic orientations of the magnetite and plagioclase: the traces of selected crystallographic planes on the thin-section surface are shown for plagioclase (black) and magnetite (white); the orientation relations between magnetite and the "Left-II" host is $(111)\,mt\,//\,(\bar{3}12)\,PL$; there is no rational orientation relation between magnetite needle and the adjacent "Left-I" twin; here $(110)\,mt$ rotates towards $(112)\,PL$, and its surface appears corroded; (C) EBSD map of the studied area: plagioclase twins (red and yellow) and "rotating" magnetite needle (from blue to green). (D) Fragment of the EBSD plot, corresponding to the EBSD map (C); rotation of $(110)\,mt$ towards $(112)\,PL$ is shown. The micro-inclusion pertains to the crystallographic orientation shown in figures 4A and 5.

and $[001]\,PL$ in all twins. In other cases single inclusions may show different crystallographic orientation relations with respect to both plagioclase twins (more or less "regular") depending on their orientation.

An example is shown in figure 6. The part of the needle that is included in one of the Carlsbad twins ("Left-I") orientations (yellow domain in fig. 6C) has a strongly corrugated interface to plagioclase, whereas the grain surface is smooth, where it is included in the "Left-I" twin orientation (red domain in fig. 6C). The $(110)\,mt$ plane in the yellow PL domain is deflected by about 5° (fig. 6D) with respect to the $(110)\,mt$ plane included in the other twin orientation (red domain in fig. 6C) toward $(112)\,PL$ of the host crystal.

*Magnetite micro-inclusions in altered plagioclase.*—In areas of chemical alteration, that is, in the OPG generation of plagioclase, near cracks, grain boundaries and hydrothermal veins, needle-shaped inclusions are often resorbed (fig. 7, see also fig. 2G). No unique crystallographic orientations were found for isolated magnetite micro-inclusions in discontinuous needles. The $[111]\,mt$ direction, which coincides with the elongation of the needles, usually maintains its orientation perpendicular to $(112)\,PL$, which also serves as a rotation axis for other magnetite inclusions in resorbed needles as shown on figure 7.
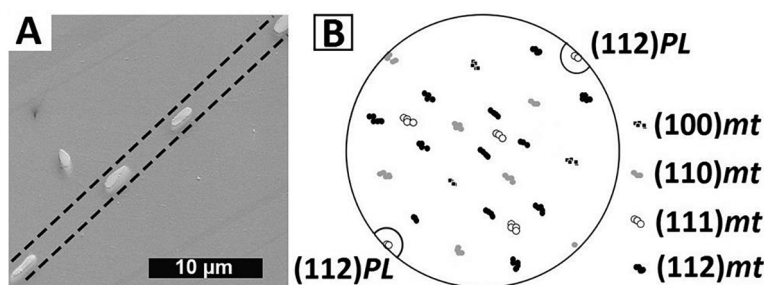
Fig. 7. (A) SE image with black dotted lines delineating the trace of a discontinuous needle; (B) pole figure plot (upper hemisphere equal angle projection) of magnetite; large circles indicate the orientation of the $(1\bar{1}2)PL$ pole, isolated parts of a needle-shaped magnetite-ilmenite micro-inclusions are rotated around a common pole $(112)PL$.

Near cracks and hydrothermal veins the micro-inclusions have less regular orientation relations with the plagioclase host. Hydrothermal plagioclase and plagioclase of the OPG assemblage is free of micro-inclusions.

*Orientation of ilmenite.*—When ilmenite forms lamellar intergrowths with magnetite (figs. 2C-2F, 2I-2K), these phases show a strong crystallographic orientation relation: (i) $(001)ilm$ parallel to one of the $(111)mt$ planes and three $(100)ilm$ parallel to three $(110)mt$ (fig. 4C); (ii) one of $(100)ilm$ parallel to one of $(110)mt$, and one of the $(110)ilm$ parallel to one of the $(111)mt$ planes.

The first one of the above described orientation regularities is the most widespread; it was observed in 95 percent of the investigated Ilm-Mt intergrowth relations. The second one was observed in some cases usually as one of several lamellae with the first type of orientation relation. The second type of orientation relation was also observed for the ilmenite lamellae spatially isolated from the previous host magnetite needle and showing signs of recrystallization (fig. 2L).

In some areas, usually in OPG plagioclase, ilmenite forms individual plates. The plates extend parallel to $(001)ilm$, and they show weak crystallographic orientation relations with plagioclase. $(001)ilm$ is approximately aligned with major plagioclase planes, whereas one of the $(100)ilm$ or $(110)ilm$ planes coincides with $(112)PL$, $(1\bar{5}0)PL$ or $(150)PL$ plagioclase planes.

It must be noted that the ilmenite lamellae are usually equally distributed with proportions of 1/6 to 1/3 in the magnetite inclusions of plagioclase of "modified gabbro". The micro-inclusions of "non-modified gabbro" do not show signs of heterogeneous phase composition.

### Chemical Compositions of Fe-Ti-oxide Micro-inclusions and Plagioclase Host

The compositions of plagioclase as determined by FEG-EMPA point analyses are given in table 2. Qualitative information on chemical compositions in and adjacent to micro-inclusions was obtained from element distribution mapping. Element maps for an ilmenite-magnetite plate hosted in relic gabbroic plagioclase (shown in fig. 2C) and for the acicular ilmenite micro-inclusions hosted in OPG-plagioclase are presented in figures 8 and 9.

The magnetite domains in the ilmenite-magnetite micro-inclusions of relic gabbroic plagioclase have close to magnetite end-member compositions (fig. 8). In the ilmenite lamellae the concentrations of manganese and magnesium are elevated relative to the concentrations of these elements in magnetite. The distribution of magnesium varies slightly between different ilmenite lamellae probably due to the presence of another non-identified sub-micron sized phase (fig. 8). The plagioclase

TABLE 2

*Chemical composition of different plagioclase generations in "modified gabbro" (wt. %)*

| generation of Pl | gabbroic | | OPG | | | | hydrothermal | | profile across ilmenite-magnetite inclusion | | | profile across ilmenite inclusion | |
|---|---|---|---|---|---|---|---|---|---|---|---|---|---|
| CL color | blue | blue | pale-red | pale-red | red | red | brown | brown | red halo | red halo | red halo | red halo | red halo |
| Analysis No | 1 | 2 | 3 | 4 | 5 | 6 | 7 | 8 | 9 | 10 | 11* | 12 | 13 |
| $SiO_2$ | 51.59 | 51.23 | 54.52 | 55.97 | 56.59 | 58.33 | 60.47 | 63.78 | 52.16 | 52.07 | 25.08* | 53.21 | 55.21 |
| $Al_2O_3$ | 29.48 | 29.40 | 27.75 | 26.03 | 26.33 | 24.55 | 23.63 | 21.29 | 29.41 | 29.40 | 15.54* | 26.69 | 24.73 |
| FeO | 0.18 | 0.32 | 0.18 | 0.27 | 0.11 | 0.25 | 0.03 | 0.01 | 0.25 | 0.40 | 51.18* | 0.17 | 0.43 |
| CaO | 13.13 | 13.18 | 10.64 | 9.09 | 9.07 | 7.23 | 5.64 | 2.81 | 13.09 | 12.91 | 6.61* | 10.07 | 8.54 |
| $Na_2O$ | 4.54 | 4.35 | 5.94 | 6.55 | 6.76 | 7.48 | 8.77 | 10.46 | 4.26 | 4.37 | 3.18* | 5.59 | 6.35 |
| $K_2O$ | 0.18 | 0.20 | 0.27 | 0.45 | 0.21 | 0.59 | 0.17 | 0.25 | 0.15 | 0.16 | 0.01* | 0.25 | 0.34 |
| $TiO_2$ | 0.03 | 0.03 | 0.01 | 0.00 | 0.01 | 0.01 | 0.02 | 0.00 | 0.03 | 0.00 | 1.36* | 0.04 | 0.24 |
| MnO | 0.00 | 0.01 | 0.01 | 0.00 | 0.00 | 0.02 | 0.00 | 0.03 | 0.01 | 0.01 | 0.05* | 0.00 | 0.01 |
| MgO | 0.01 | 0.01 | 0.00 | 0.03 | 0.00 | 0.02 | 0.00 | 0.00 | 0.03 | 0.04 | 0.06* | 0.00 | 0.03 |
| Total | 99.14 | 98.73 | 99.32 | 98.39 | 99.08 | 98.48 | 98.73 | 98.63 | 99.39 | 99.36 | 103.07* | 96.02 | 95.88 |
| | | | | | | formula units | | | | | | | |
| Si | 2.35 | 2.35 | 2.46 | 2.55 | 2.55 | 2.64 | 2.71 | 2.83 | 2.38 | 2.38 | - | 2.49 | 2.59 |
| Al | 1.59 | 1.59 | 1.48 | 1.40 | 1.40 | 1.31 | 1.25 | 1.12 | 1.58 | 1.58 | - | 1.47 | 1.36 |
| Fe | 0.007 | 0.012 | 0.007 | 0.010 | 0.004 | 0.009 | 0.001 | 0.000 | 0.010 | 0.015 | - | 0.007 | 0.017 |
| Ca | 0.64 | 0.65 | 0.52 | 0.44 | 0.44 | 0.35 | 0.27 | 0.13 | 0.64 | 0.63 | - | 0.50 | 0.43 |
| Na | 0.40 | 0.39 | 0.52 | 0.58 | 0.59 | 0.66 | 0.76 | 0.90 | 0.38 | 0.39 | - | 0.51 | 0.58 |
| K | 0.011 | 0.011 | 0.015 | 0.026 | 0.012 | 0.034 | 0.010 | 0.014 | 0.009 | 0.010 | - | 0.015 | 0.020 |
| Ti | 0.001 | 0.001 | 0.000 | 0.000 | 0.000 | 0.000 | 0.001 | 0.000 | 0.001 | 0.000 | - | 0.001 | 0.008 |
| Mn | 0.000 | 0.000 | 0.000 | 0.000 | 0.000 | 0.001 | 0.000 | 0.001 | 0.000 | 0.000 | - | 0.000 | 0.000 |
| Mg | 0.000 | 0.001 | 0.000 | 0.002 | 0.000 | 0.001 | 0.000 | 0.000 | 0.002 | 0.003 | - | 0.000 | 0.002 |
| An# | 62 | 63 | 50 | 43 | 43 | 35 | 26 | 13 | 63 | 62 | 53 | 50 | 43 |
| Na/(Si+Al) | 0.102 | 0.100 | 0.132 | 0.147 | 0.149 | 0.167 | 0.192 | 0.228 | 0.096 | 0.098 | 0.142 | 0.128 | 0.147 |

Note. (*) an. 11 represents a mixed analysis of plagioclase and magnetite. Analyses 10 and 13 correspond to areas in immediate proximity to the micro-inclusions.
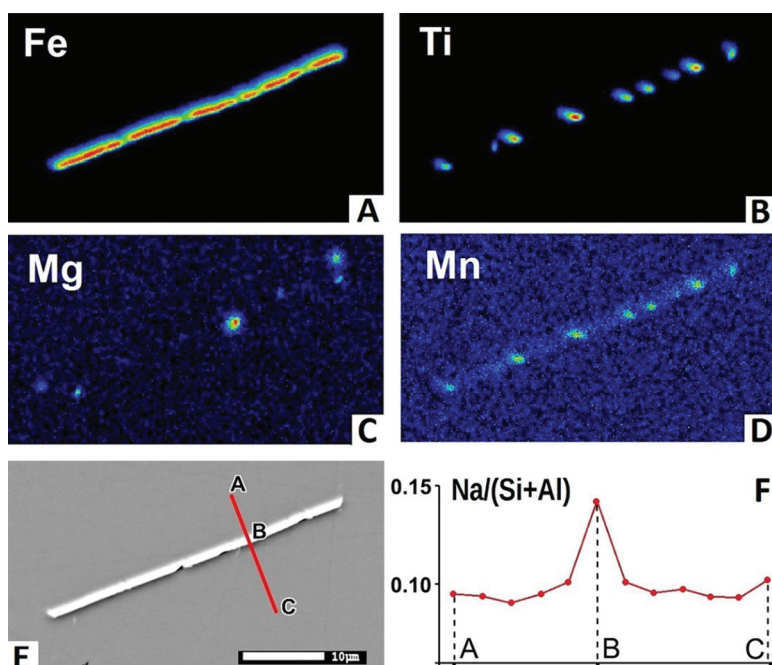
Fig. 8. Element map of ilmenite-magnetite micro-inclusion in relic gabbroic plagioclase: (A) – Fe; (B) – Ti; (C) – Mg; (D) – Mn; (E) – SE image and (F) compositional profile of Na/(Si+Al) ratio along the profile line with reference points *A*, *B* and *C* indicated in figure (E).

host is calcic (table 2, analyses 9-10). Towards the magnetite-ilmenite inclusion a subtle increase in Na/(Si+Al) ratios was detected within an about 5 micrometers wide zone by means of line scans (table 2, analysis 10).

The area surrounding an ilmenite needle in the transition zone from relic gabbroic to OPG-plagioclase (An63-50) shows a more complex mineral assemblage (figs. 9 and 10). Additional phases were identified at the interface between ilmenite inclusion and plagioclase host. Based on chemical composition and appearance in transmitted light and on BSE images amphibole (Ca, Mg, Fe, Si and Al), biotite (K, Mg, Fe, Si, Al), and potassium feldspar (K, Si, Al) were discerned. Moreover, the concentration of Na in Pl increases and the concentration of Ca decreases towards the ilmenite inclusion within an about 5 micrometers wide zone in the plagioclase host. The anorthite content decreases down to $An_{42}$ in the immediate proximity to the ilmenite plate (fig. 10). This composition change correlates with an increase of the potassium concentration in plagioclase (fig. 10). This is in line with the appearance of potassium-bearing minerals at the interface between ilmenite and plagioclase.

The most pronounced composition change of plagioclase is an increase of the Na content in areas surrounding the micro-inclusions. This composition halo is also reflected by CL luminescence: the micro-inclusions in "modified gabbro" in most cases have a red CL halo whose configuration and color intensity correlate with the distribution and composition of sodium-rich domains in plagioclase (fig. 10).

The correlation between CL color and chemical composition of plagioclase is shown in figure 11. Calcic plagioclase with $An_{65-55}$ (fig. 11A), which is considered as primary magmatic relic gabbroic plagioclase exhibits light blue luminescence; the CL color of OPG related plagioclase varies from pale-red ($An_{50-43}$) to red ($An_{43-35}$) and
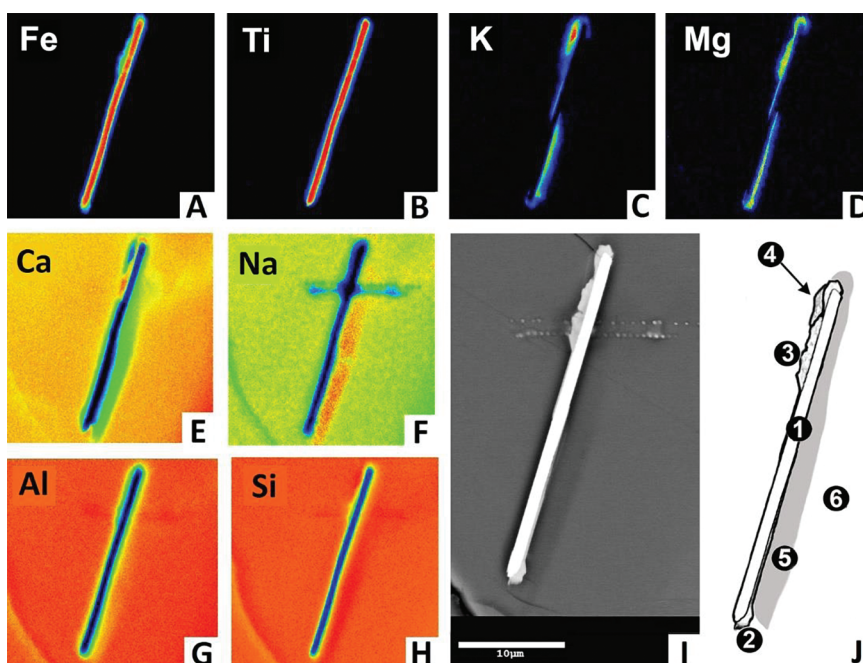
Fig. 9. Element distribution map for ilmenite micro-inclusion in the OPG generation of plagioclase (A – H), SEM image (I) and schematic drawing of phases distribution (J): 1 – ilmenite; 2 – biotite; 3 – amphibole; 4 – potassium feldspar; 5 – sodic plagioclase; 6 – calcic plagioclase.

dark red ($An_{35-32}$); the hydrothermally altered plagioclase ($An_{26-13}$) has dark red-brown luminescence through which it can be distinguished from plagioclase filling voids in hydrothermal veins, which show bright red luminescence (fig. 1).

The CL-color varieties of plagioclase form distinct groups following consistent trends with respect to their K/An# and Fe/Ca ratios (fig. 11). The OPG plagioclase shows the highest potassium concentrations. The increase of K contents in plagioclase surrounding ilmenite plates (figs. 9, 10 and 11A) is in accordance with this OPG trend.

The distribution of iron in plagioclase surrounding micro-inclusions is of particular interest. The concentration of $FeO_T$ in plagioclase including ilmenite micro-inclusion increases from 0.17 to 0.43 weight percent (fig. 10) at a distance of about 5 to 10 micrometers from the inclusion (the Fe content obtained from domains less than 5
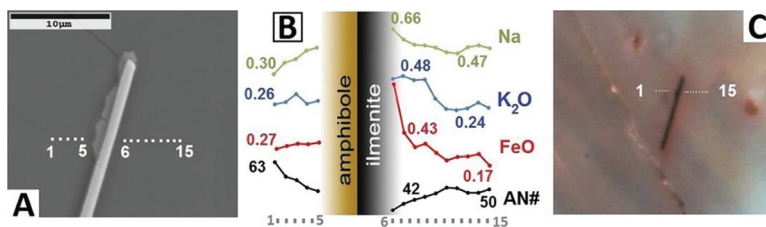


Fig. 10. Ilmenite micro-inclusion hosted in the OPG generation of plagioclase (fig. 9): SE (A), CL (C) images and microprobe point analyses along a profile across the ilmenite needle and into the plagioclase host on both sides of the needle (B); element contents are given as atoms per formula units (for Na) and wt.% (for $K_2O$ and FeO).
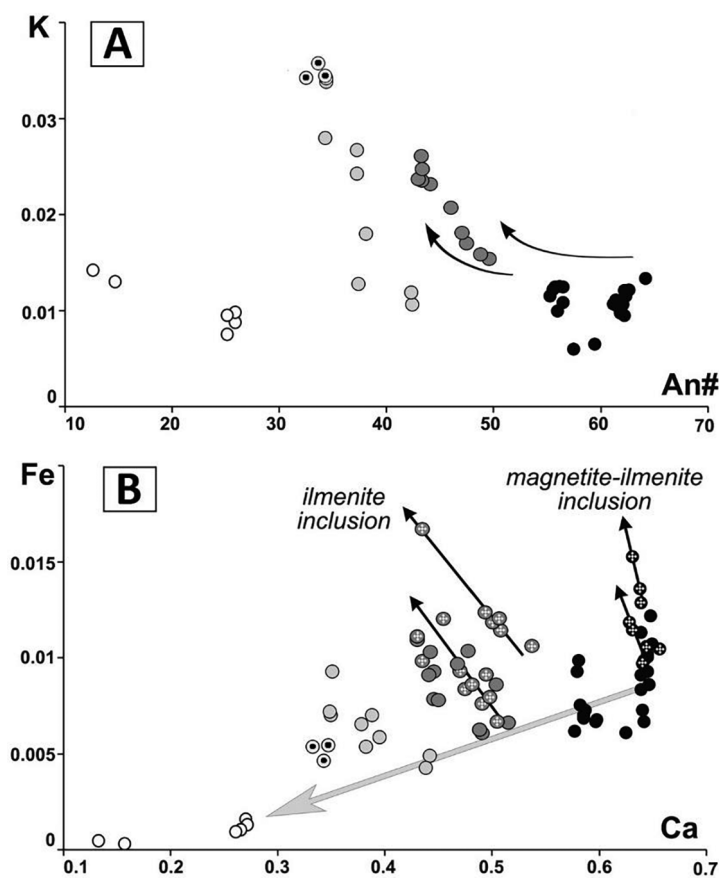
Fig. 11. K(f.u.)/An# (A) and Fe(f.u.)/Ca(f.u.) (B) Ratios in different genetic groups of plagioclase, characterized by specific CL-colors: gabbroic plagioclase with blue CL (black circles); OPG plagioclase with pale-red CL (dark gray circles), OPG plagioclase with intensive red CL (gray circles) and OPG plagioclase with dark red CL (gray circles with black dots); hydrothermal plagioclase with brown CL (white circles); black arrows indicate chemical alteration trends of plagioclase towards the ilmenite plate (A); and ilmenite and ilmenite-magnetite plates (B); white crosses indicate microprobe analysis taken from corresponding profiles across micro-inclusions; gray arrow indicates general trend of plagioclase evolution from gabbroic via OPG to hydrothermal generations.

micrometers from an inclusion have not been reported due to potential influence of Fe fluorescence from the Fe-rich inclusion). In general, the Fe-content is positively correlated with the Na- and negatively correlated with the Ca content of plagioclase (fig. 11B). These composition trends differ from the general chemical evolution trend from relict gabbroic to OPG and hydrothermal plagioclase where Fe and Ca contents are positively correlated (fig. 11B).

DISCUSSION

A consistent chemical and microstructural evolution of the Fe-Ti-oxide micro-inclusions and plagioclase host during successive magmatic and hydrothermal stages of the gabbro-plagiogranite association of the Mid-Atlantic ridge at 13°34' N has been established. The first generation of micro-inclusions is represented by abundant extremely fine-grained, dust-like magnetite inclusions and magnetite needles with strong shape preferred orientation in primary magmatic plagioclase of gabbroic rocks.

The shape orientation of the magnetite needles does not show simple relations with the lattice of the host plagioclase such as parallel orientation to main crystallographic directions like cleavage- and habit planes or twin orientations. This excludes formation by overgrowth of Fe-Ti-oxides floating in a melt by plagioclase, because in such case the shape orientation of the inclusion would be expected to be related to typical growth facets of plagioclase. The observed rational crystallographic orientation relation with [112] magnetite parallel to [4$\bar{3}$5] plagioclase and corresponding (110) magnetite parallel to (131) plagioclase (see fig. 3) indicates that the Fe-Ti-oxide inclusions used the crystal structure of plagioclase as a template for crystallization. Two scenarios are conceivable: The Fe-Ti-oxides may have nucleated heterogeneously and grown on the advancing growth surfaces of plagioclase and were subsequently overgrown by the plagioclase. Alternatively the Fe-Ti-oxide inclusions may have formed by precipitation from super-saturated iron-bearing plagioclase under sub-solidus conditions. Their appearance possibly was related to the presence of water, which may catalyze clouding of plagioclase under sub-solidus conditions (Smith, 1974). We suppose that the first generation magnetite precipitates had appreciable titanium contents, which influenced their subsequent microstructure and texture evolution. Henceforth the term titanomagnetite will be used to describe these early stage precipitates.

During the OPG-stage the gabbro was intruded by quartz-biotite veinlets. Based on the close spatial correlation between re-crystallized Fe-Ti-oxide micro-inclusions and plagiogranite mineralization, the transformation of primary dust-like and needle-shaped titanomagnetite micro-inclusions to more coarse-grained ilmenite-magnetite lamellar intergrowths forming needles, ossicles and plates is ascribed to this event.

Magnetite is the volumetrically dominant phase in the lamellar magnetite-ilmenite intergrowth that emerged from the original extremely fine-grained titanomagnetite micro inclusion. It has complex but rational orientation relations to the plagioclase host, which are, in part, inherited from the original orientation relation between primary titanomagentite inclusions and the plagioclase host. More specifically, this applies to the parallel orientation of magnetite (110) and plagioclase (131), which was identified for both studied gabbroic titanomagnetite and for the majority of magnetite from "modified gabbro" (figs. 3 and 4B). In addition, other crystallographic and shape orientations have developed in the micro inclusions in "modified gabbro". The elongation of the needle shaped inclusion in "modified gabbro" coincides with: (i) magnetite [111] which is parallel to the poles of plagioclase (11$\bar{2}$) and (1$\bar{5}$0); (ii) magnetite [110] may rotate freely within plagioclase (11$\bar{2}$) and (1$\bar{5}$0) with preferred orientation parallel to plagioclase [001] which is contained in plagioclase (1$\bar{5}$0). Similar shape preferred orientations of Fe-Ti-oxide micro-inclusion related to the (11$\bar{2}$) and (1$\bar{5}$0) planes and the [001]-direction in plagioclase have been found earlier based on optical observation (Andersen, 1915; Divljan, 1960; Kraeft and Saalfeld, 1967; Popov and others, 1978; Sobolev, 1990).

*Origin of Crystallographic Orientation Relations between Magnetite and Plagioclase Host*

It is commonly observed that layers and directions of densely packed oxygen control epitactic and topotactic orientation relations. This reasoning is demonstrated with comparatively simple crystal structures such as periclase, spinel and corundum in the MgO-Al$_2$O$_3$ chemical system (for example Jeřábek and others, 2014). Such reasoning is less obvious for the more complex situation encountered at the interfaces between the framework structure of triclinic plagioclase and cubic magnetite. Nevertheless, the plagioclase crystal structure contains layers of oxygen parallel to its (11$\bar{2}$) and (1$\bar{5}$0) planes. The angle between these two planes is close to 90°. In the predominant case of the observed orientation relations the magnetite (111) and (110) planes, which contain densely packed oxygen layers, are parallel to these plagioclase lattice planes. This is why we suggest that parallel orientation of oxygen layers in the Fe-Ti-oxide

precipitates and in the plagioclase host probably determines the main crystallographic orientation relations between the host and micro-inclusions in "modified gabbro". Furthermore, there a good lattice match exists between the magnetite (111) plane and some prominent plagioclase planes. The d-spacing of magnetite (222) is 2.42 Å. This is close to $(112)PL$=2.46 Å, $(1\bar{5}0)PL$=2.43 Å, $(150)PL$=2.40 Å, and $(\bar{3}12)PL$=2.50 Å. Also the magnetite (110) plane shows a match with some plagioclase planes: the d-spacing is 2.97 Å for magnetite (220), which is close to $(131)PL$=2.84 Å and $(04\bar{1})PL$= 2.94 Å. It must be noted, however, that another frequently observed orientation relation, $(110)mt$ parallel to $[001]PL$ cannot be explained by matching lattice parameters: lattice vector along Pl[001] is 7.14 Å which is not a multiple of the magnetite (110) d-spacing.

### Origin of Deviations from the Main Orientation Relations

Deviations from the main orientation relations may result from different factors. Firstly, twinning in plagioclase may lead to repetition of orientation relations with only slight misorientation. For example, $(\bar{3}12)$ of "Left-II" twin is nearly parallel to (112) of the "Right-I" orientation; similarly $(1\bar{5}0)$ of one albite twin is parallel to (150) of the other one. In our study Fe-Ti-oxide micro-inclusion were found to pertain to all these variants (table 1, fig. 5). Orientation relations and twinning in plagioclase have been addressed earlier (Sobolev, 1990). Observed relations may indicate relict orientation relations, which were established before plagioclase twinning. Alternatively the needles may have nucleated in one of the twins and grown into the adjacent one. Indeed, the structure of plagioclase shows that $(\bar{3}12)$ and (150) plagioclase planes have close to (112) and $(1\bar{5}0)$ correspondence between twins.

Moreover, needle- or plate-shaped Fe-Ti-oxide micro-inclusions are deflected and show changes in their shape- and crystallographic orientation at twin boundaries. In the case presented in figure 6A plate of magnetite extends across an albite twin boundary. In one twin magnetite (111) is parallel to plagioclase (-312), whereas in the other plagioclase twin the two lattices are far from this orientation relation. At the twin boundary the magnetite grain bends in such a way that the orientation of magnetite (110) approaches but does not reach the orientation of plagioclase (112). The EBSD map in figure 6C reveals constant orientation of the magnetite portion hosted in twin "Left-II" and a gradual orientation change in the portion that is hosted in twin "Left-I". This suggests that magnetite originally nucleated and grew in twin "Left-II" with the favorable orientation relation given by magnetite (111) parallel to plagioclase (-312). Only when it hits twin "Left-I", the densely packed oxygen layers of magnetite were no more in a favorable orientation with respect to the oxygen layers in the plagioclase host. The lattice of magnetite seems to have been "attracted" by the now differently oriented lattice of the plagioclase host such that a new favorable orientation relation with magnetite (110) parallel to plagioclase (112) is approached as is indicated by the rotation of the magnetite (110) pole towards the plagioclase (112) pole (fig. 6D).

Another phenomenon of minute misorientation was observed where gabbroic plagioclase was modified during the OPG or the hydrothermal stage. There, magnetite needles separated into individual, strictly aligned grains that slightly changed their lattice orientation during the separation process (fig. 7). Based on the fact that the "rotation" of the lattice orientations of magnetite micro-inclusions of groups "$1_{rot}$" and "$2_{rot}$" on figure 4B, around a common axis follows the same trend (same rotation axis) as the development of slight misorientation due to twinning and/or recrystallization in "modified gabbro" we infer that these two phenomena are related. It is important to note that albite-twinned plagioclase is prominent in "modified gabbro" but is hardly ever observed in "non-modified gabbro". This suggests that albite twinning is potentially related to tectonic movement or pressure related to OPG intrusion.

Finally, the group of the micro-inclusions with less widespread or single orientation (see table 1, right column) exhibits orientation relations to main planes of the plagioclase structure (for example cleavage and twining planes, crystal faces *et cetera*) and to directions along which the plagioclase structure contains channels in the framework of Si, Al- tetrahedra. Some of these orientation relations were described from metamorphic rocks by Wenk and others (2011). It was suggested by the latter authors that channels in the Si, Al- tetrahedral framework may control the evolution of habit planes of precipitates. In our samples micro-inclusions of this group are observed on twin boundaries, in areas surrounding OPG veins, and in the rims of the grains suggesting formation during late stage re-crystallization.

### Late Stage Alteration of Inclusion Host Assemblages

According to phase relations in the Fe-Ti-O system (Sauerzapf and others, 2008) the transformation of titanomagnetite into ilmenite-magnetite intergrowth may be driven by oxidation. An example of such a situation in granulites was presented by Degi and others (2009). In our samples this transformation is prominent only in the domains of "modified gabbro" indicating that the alteration stages following primary crystallization of the gabbro occurred in a relatively more oxidizing environment.

The anorthite content and Fe concentrations of plagioclase decrease from the gabbroic to the hydrothermal stage (fig. 11B). Furthermore, the Na and K contents increase during the OPG- stage, but they show different behavior in the hydrothermal stage with continued increase of the Na- and distinct decrease of the K contents. On top of this general trend, plagioclase is chemically altered in the immediate vicinity to Fe-Ti-oxide micro-inclusions, where the anorthite content generally decreases and the contents of Fe and K increase relative to the bulk of the plagioclase host. The composition of melt inclusions from the same sample of modified gabbro (Aranovich and others, 2015) show that the granite melt was K-rich. The enrichment of K in plagioclase surrounding ilmenite, as well as the appearance of K-bearing minerals at the interface between ilmenite plates and plagioclase host thus indicate that formation of homogeneous ilmenite was related to the OPG stage.

Halos with elevated albite content and increased Fe concentrations in plagioclase surrounding magnetite-ilmenite and ilmenite plates (see figs. 9 and 10) are characterized by red cathodoluminescence (fig. 10). Concomitant increase of Na and Fe content is inversely related with the general trend in plagioclase compositions from the gabbroic to the hydrothermal stage. It has been shown (Hofmeister and Rossman, 1984) that $Fe^{2+}$ substitutes for Ca, and the anorthite content is an important factor controlling the partitioning of divalent iron into plagioclase. In contrast, $Fe^{3+}$ is tetrahedrally coordinated in plagioclase and replaces Al. In any case, a positive correlation between Fe- and anorthite content is naturally expected and was indeed documented repeatedly for natural sodic and intermediate plagioclases (Smith, 1983) (fig. 11B).

The inverse correlation between anorthite- and Fe-content in plagioclase surrounding the micro-inclusions is unusual. Similar inverse Fe/An# correlation was described in plagioclase of ferrodiorites of the Skaergaard intrusion (Tegner, 1997), where the concomitant enrichment of plagioclase in Fe, Si and Na was ascribed to the increase of iron content in the magma due to fractionation.

In the case at hand, two mechanisms must be considered that lead to formation of the chemically altered halos. On the one hand, the interfaces between the Fe-Ti-oxide micro inclusions and the plagioclase host served as preferred passageways for fluids. This has been demonstrated for secondary alteration of perthites along precipitate-host interfaces (Abart and others 2009a, 2009b; Tajcmanova and others 2012). The fluids associated with the OPG event penetrated into the plagioclase preferentially along the precipitate-plagioclase interfaces and supplied Na and Si to plagioclase and
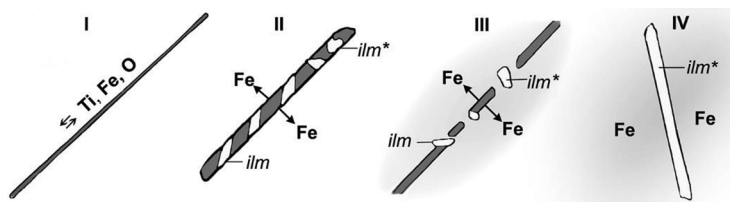
Fig. 12. Microstruture evolution of the Fe-Ti-oxide micro-inclusions in the plagioclase of "modified gabbro": I – titanomagnetite micro-inclusion; II – magnetite-ilmenite inclusion with ilmenite lamellae of usual (ilm) orientation relations: $(001)ilm$ // $(111)mt$ and rare (ilm*) orientation relations: $(110)ilm$ // $(111)mt$; III – discontinuous magnetite – ilmenite inclusions with ilm* orientation of separated ilmenite lamellae and forming Fe,Na – alteration halo; IV – recrystallized ilmenite surrounded by Fe,Na,Si – halo.

also affected the magnetite micro-inclusions. On the other hand, Fe was leached from the micro-inclusions and supplied to the surrounding plagioclase host. Selective resorption of magnetite from magnetite-ilmenite micro-inclusions is indicated by thinning of magnetite, while ilmenite was largely preserved (fig. 2L).

Subsequent growth of ilmenite is indicated by a change of its crystallographic orientation relation to the plagioclase host. Initially, ilmenite-magnetite inclusions and plagioclase host show orientation relations with $(001)ilm$ parallel to $(111)mt$, which in turn is parallel to $(112)PL$ or $(1\bar{5}0)PL$ of the host (*Ilm* in fig. 12, II and III). However, isolated (fig. 12, II) or disconnected (fig. 12, III) ilmenite lamellae from discontinuous magnetite-ilmenite inclusions, and isolated homogeneous ilmenite plates (fig. 12, IV) show orientation relations with $(110)ilm$ parallel $(111)mt$, and $(110)ilm$ or $(100)ilm$ parallel to $(112)PL$ or $(150)PL$ of the host, which differ from the usual scheme. These orientation relations possibly correspond to the lowest energy configuration for an ilmenite precipitate in a plagioclase matrix, which was only attained during re-crystallization of ilmenite in contact with the lattice of the plagioclase host.

The hydrothermal generation of plagioclase is characterized by low An# and Fe content (fig. 11 and table 2) and does not contain any type of micro-inclusions pointing to the completion of the micro-inclusion evolution following "cleaning" of the plagioclase from Fe.

The revealed microstructural evolution of the micro-inclusions and the plagio-clase host is in accordance with earlier established petrological evolution of the studied rocks (Pertsev and others, 2012; Aranovich and others, 2015).

CONCLUSIONS

The microstructural, textural and chemical evolution of microcrystalline Fe-Ti-oxide inclusions and plagioclase host in a gabbro-plagiogranite assemblage from the Mid-Atlantic ridge at 13°34' N has been investigated using optical microscopy and electron beam micro-analytical techniques. Based on the combined evidences we suggest the following formation history (fig. 12). The first evolution stage is repre-sented by abundant, extremely fine grained dust-like inclusions of titanomagnetite in primary magmatic plagioclase. Most likely titanomagnetite formed by precipitation from plagioclase, which had become super-saturated with respect to Fe-Ti-oxide either by cooling or, alternatively, by oxidation. In any case, precipitation took place at sub-solidus conditions.

Subsequent transformation of titanomagnetite to more coarse-grained magnetite-ilmenite intergrowths was associated with the intrusion of oceanic plagiogranite. The original shape and crystallographic orientation relations between first generation titanomagnetite and plagioclase host were partially preserved during this transforma-tion. In addition a multitude of new rational orientation relations were established,

which were primarily controlled by parallel orientation of densely packed oxygen layers of the Fe-Ti-oxides with oxygen layers of the plagioclase structure and/or by good matching of lattice vectors between two crystal structures. During further evolution magnetite was selectively dissolved leaving behind isolated ilmenite plates or needles, which underwent re-crystallization including a slight change in their crystal orientation relations to the host plagioclase. Alteration halos enriched in Si, Na, K, and Fe and depleted in Al and Ca relative to the bulk plagioclase developed around Fe-Ti-oxide inclusions during this stage. Twinning of host plagioclase and recrystallization of the Fe-Ti-oxide micro-inclusions lead to minute but systematic changes of the host-inclusion orientation relations explaining the overall variability of observed orientation relations. Finally, hydrothermal alteration produced plagioclase that is entirely free of micro-inclusions. The Fe-Ti-oxide micro-inclusions are the main carriers of the paleo-magnetics signature of these rocks. The mechanisms of their primary formation as well as subsequent transformation and alteration may potentially influence their paleo-magnetic record. With this study we provide a petrographic frame as reference for paleo-magnetic data from the ocean floor.

## ACKNOWLEDGMENTS

## REFERENCES

Abart, R., Petrishcheva, E., Käβner, S., and Milke, R., 2009a, Perthite microstructure in magmatic alkali feldspar with oscillatory zoning; Weinsberg Granite, Upper Austria: Mineralogy and Petrology, v. 97, n. 3, p. 251–263, http://dx.doi.org/10.1007/s00710-009-0090-1

Abart, R., Petrishcheva, E., Wirth, R., and Rhede D., 2009b, Exsolution by spinodal decomposition: II: Perthite formation during slow cooling of anatexites from Ngornghoro, Tanzania: American Journal of Science, v. 309, n. 6, p. 450–475, http://dx.doi.org/10.2475/06.2009.02

Armbrustmacher, T. J., and Banks, N. G., 1974, Clouded plagioclase in metadolerite dikes, southeastern Bighorn Mountains, Wyoming: American Mineralogist, v. 59, n. 7–8, p. 656–665.

Andersen, O., 1915, On aventurine feldspar: American Journal of Science, Fourth series, v. 40, n. 238, p. 351–399, http://dx.doi.org/10.2475/ajs.s4-40.238.351

Anderson, A. T., Jr., 1966, Mineralogy of the Labrieville anorthosite, Quebec: American Mineralogist, v. 51, n. 11–12, p. 1671–1711.

Aranovich, L. Ya., Prokofiev, V. Yu., Pertsev, A. N., Bortnikov, N. S., Ageeva, O. A., Bel'tenev, V. E., and Simakin, S. G., 2015, Composition and origin of a $K_2O$ rich granite melt in the Mid Atlantic Ridge, 13° 34′ N: Evidence from the analysis of melt inclusions and minerals of the gabbro–plagiogranite association: Doklady Earth Sciences, v. 460, n. 2, p. 174–178, http://dx.doi.org/10.1134/S1028334X15020166

Bolle, O., Diot, H., and Trindade, R. I. F., 2003, Magnetic fabrics in the Holum granite (Vest-Agder, southernmost Norway): implications for the late evolution of the Sveconorwegian (Grenvillian) orogen of SW Scandinavia: Precambrian Research, v. 121, n. 3–4, p. 221–249, http://dx.doi.org/10.1016/S0301-9268(03)00013-5

Bottinga, Y., Kudo, A., and Weill, D., 1966, Some observations on oscillatory zoning and crystallization of magmatic plagioclase: American Mineralogist, v. 51, n. 5–6, p. 792–806.

Bridgewater, D., and Harry, W. T., 1968, Anorthosite xenoliths and plagioclase megacrysts in Precambrian intrusion of South Greenland: Meddelelser om Grønland, v. 185, p. 1–243.

Carstens, H., 1955, On the clouding of plagioclase in coronited metadolerites: Norsk Geologisk Tidsskrift, v. 35, p. 129–134.

Cottrell, R. D., and Tarduno, J. A., 1999, Geomagnetic paleointensity derived from single plagioclase crystals: Earth and Planetary Science Letters, v. 169, n. 1–2, p. 1–5, http://dx.doi.org/10.1016/S0012-821X(99)00068-0

Davis, K. E., 1981, Magnetite rods in plagioclase as the primary carrier of stable NRM in ocean floor gabbros: Earth and Planetary Science Letters, v. 55, n. 1, 190–198, http://dx.doi.org/10.1016/0012-821X(81)90098-4

Dégi, J., Abart, R., Török, K., Rhede, D., and Petrishcheva, E., 2009, Evidence for xenolith–host basalt interaction from chemical patterns in Fe–Ti-oxides from mafic granulite xenoliths of the Bakony–

Balaton Volcanic field (W-Hungary): Mineralogy and Petrology, v. 95, n. 3, p. 219–234, http://dx.doi.org/10.1007/s00710-008-0035-0

Diot, H., Bolle, O., Lambert, J. M., Launeau, P., and Duchesne, J. C., 2003, The Tellnes ilmenite deposit (Rogaland, South Norway): magnetic and petrofabric evidence for emplacement of a Ti-enriched noritic crystal mush in a fracture zone: Journal of Structural Geology, v. 25, n. 4, p. 481–501, http://dx.doi.org/10.1016/S0191-8141(02)00050-0

Divljan, S., 1960, The results of field and laboratory studies of aventurine plagioclases from some Norwegian pegmatites: Proceedings of the 21st International Geological Congress, Norden, v. 17, p. 94–101.

Evans, M. E., and McElhinny, M. W., 1966, The paleomagnetism of the Modipe gabbro: Journal of Geophysical Research, v. 71, n. 24, p. 6053–6063, http://dx.doi.org/10.1029/JZ071i024p06053

Feinberg, J. M., Scott, G. R., Renne, P. R., and Wenk, H. R., 2005, Exsolved magnetite inclusions in silicates: Features determining their remanence behavior: Geology, v. 33, n. 6, p. 513–516, http://dx.doi.org/10.1130/G21290.1

Fleet, M. E., 1982, Orientation of phase and domain boundaries in crystalline solids: American Mineralogist, v. 67, n. 9–10, p. 926–936.

Hargraves, R. B., and Young, W. M., 1969, Source of stable remanent magnetism in Lambertville diabase: American Journal of Science, v. 267, n. 10, p. 1161–1177, http://dx.doi.org/10.2475/ajs.267.10.1161

Hargraves, R. B., Briden, J. C., and Daniels, B. A., 1999, Palaeomagnetism and magnetic fabric in the Freetown Complex, Sierra Leone: Geophysical Journal International, v. 136, n. 3, p. 705–713, http://dx.doi.org/10.1046/j.1365-246x.1999.00760.x

Hofmeister, A. M., and Rossman, G. R., 1984, Determination of $Fe^{3+}$ and $Fe^{2+}$ concentrations in feldspar by optical absorption and EPR spectroscopy: Physics and Chemistry of Minerals, v. 11, n. 5, p. 213–224, http://dx.doi.org/10.1007/BF00308136

Jeřábek, P., Abart, R., Rybacki, E., and Habler, G., 2014, Microstructure and texture evolution during growth of magnesio-aluminate spinel at corundum–periclase interfaces under uniaxial load: The effect of stress concentration on reaction progress: American Journal of Science, v. 314, n. 5, p. 940–965, http://dx.doi.org/10.2475/05.2014.02

Kraeft, U., and Saalfeld, H., 1967, Über die Aventurin-Oligoklase von Tvedestrand und Bjordam (Norwegen): Schweizerische mineralogische und petrographische Mitteilungen, v. 47, n. 1, p. 247–256.

MacGregor, A. G., 1931, Clouded feldspars and thermal metamorphism: Mineralogical Magazine, v. 22, n. 133, p. 524–538, http://dx.doi.org/10.1180/minmag.1931.022.133.05

McClay, K. R., 1974, Single-domain magnetite in the Jimberlana norite, Western Australia: Earth and Planetary Science Letters, v. 21, n. 4, p. 367–376, http://dx.doi.org/10.1016/0012-821X(74)90175-7

Morgan, G. E., and Smith, P. P. K., 1981, Transmission electron microscope and rock magnetic investigations of remanence carriers in a Precambrian metadolerite: Earth and Planetary Science Letters, v. 53, n. 2, p. 226–240, http://dx.doi.org/10.1016/0012-821X(81)90156-4

Murthy, G. S., Evans, M. E., and Gough, D. I., 1971, Evidence of single-domain magnetite in the Michikamau anorthosite: Canadian Journal of Earth Sciences, v. 8, n. 3, p. 361–370, http://dx.doi.org/10.1139/e71-036

Nakamura, N., and Nagahama, H., 2001, Changes in magnetic and fractal properties of fractured granites near the Nojima Fault, Japan: Island Arc, v. 10, n. 3–4, p. 486–494, http://dx.doi.org/10.1111/j.1440-1738.2001.00347.x

Pertsev, A. N., Bortnikov, N. S., Vlasov, E. A., Beltenev, V. E., Dobretsova, I. G., and Ageeva, O. A., 2012, Recent massive sulfide deposits of the Semenov ore district, Mid-Atlantic Ridge, 13° 31′ N: Associated rocks of the oceanic core complex and their hydrothermal alteration: Geology of Ore Deposits, v. 54, n. 5, p. 334–346, http://dx.doi.org/10.1134/S1075701512050030

Philpotts, A. R., 1966, Origin of the anorthosite-mangerite rocks in southern Quebec: Journal of Petrology, v. 7, n. 1, p. 1–64, http://dx.doi.org/10.1093/petrology/7.1.1

Poldervaart, A., and Gilkey, A. K., 1954, On clouded plagioclase: American mineralogist, v. 39, n. 1–2, p. 75–91.

Popov, V. A., Polyakov, V. O., Bragin, N. P., and Levanov, A. A., 1978, The sunstone from Northen part of Ilmeny Mountains, *in* Popov, V. A., and Kornilov, U. B., editors, Investigations of mineralogy and geochemistry of the Urals: AN USSR, Ural Scientific Center, p. 65–69 (in Russian).

Renne, P. R., and Onstott, T. C., 1988, Laser-selective demagnetization: A new technique in paleomagnetism and rock magnetism: Science, v. 242, n. 4882, p. 1152–1155, http://dx.doi.org/10.1126/science.242.4882.1152

Renne, P. R., Scott, G. R., Glen, J. M. G., and Feinberg, J. M., 2002, Oriented inclusions of magnetite in clinopyroxene: Source of stable remanent magnetization in gabbros of the Messum Complex, Namibia: Geochemistry, Geophysics, Geosystems, v. 3, n. 12, p. 1–11, http://dx.doi.org/10.1029/2002GC000319

Reynolds, D. L., 1936, The two monzonitic series of the Newry Complex: Geological Magazine, v. 73, n. 8, p. 337–364.

——— 1946, The sequence of geochemical changes leading to granitization: Quarterly Journal of the Geological Society, v. 102, n. 1–4, p. 389–446, http://dx.doi.org/10.1144/GSL.JGS.1946.102.01-04.17

Sauerzapf, U., Lattard, D., Burchard, M., and Engelmann, R., 2008, The titanomagnetite–ilmenite equilibrium: New experimental data and thermo-oxybarometric application to the crystallization of basic to intermediate rocks: Journal of Petrology, v. 49, n. 6, p. 1161–1185, http://dx.doi.org/10.1093/petrology/egn021

Selkin, P. A., Gee, J. S., Tauxe, L., Meurer, W. P., and Newell, A. J., 2000, The effect of remanence anisotropy on paleointensity estimates: a case study from the Archean Stillwater Complex: Earth and Planetary Science Letters, v. 183, n. 3, p. 403–416, http://dx.doi.org/10.1016/S0012-821X(00)00292-2

Sengupta, P., and Ray, A., 2012, Newer Dolerite dykes, Jharkhand, India: a case study of magma generation,

differentiation and metasomatism in a subduction zone setting: Geochemical Journal, v. 46, n. 6, p. 477–491, http://dx.doi.org/10.2343/geochemj.1.0174

Smirnov, A. V., Tarduno J. A., and Pisakin B. N., 2003, Paleointensity of the Early Geodynamo (2.45 Ga) as Recorded in Karelia: A Single Crystal Approach: Geology, v. 31, n. 5, p. 415–418, http://dx.doi.org/10.1130/0091-7613(2003)031<0415:POTEGG>2.0.CO;2

Smith, J. V., 1974, Feldspar Minerals, Volume 2, Chemical and Textural Properties: Berlin, Springer-Verlag, 690 p.

—— 1983, Phase equilibria of plagioclase, *in* Ribbe, P. H., editor, Feldspar mineralogy, 2nd edition: Reviews in Mineralogy, v. 2, p. 223–239

Sobolev, P. O., 1990, Orientation of acicular iron-ore mineral inclusions in plagioclase: International Geology Review, v. 32, n. 6, p. 616–628, http://dx.doi.org/10.1080/00206819009465804

Tajcmanova, L., Abart, R., Wirth, R., Habler, G., and Rhede, D., 2012, Intracrystalline microstructures in alkali feldspars from fluid-deficient felsic granulites: a mineral chemical and TEM study: Contributions to Mineralogy and Petrology, v. 164, n. 4, p. 715–729, http://dx.doi.org/10.1007/s00410-012-0772-2

Tarduno, J. A., Cottrell, R. D., and Smirnov, A. V., 2006, The paleomagnetism of single silicate crystals: Recording geomagnetic field strength during mixed polarity intervals, superchrons, and inner core growth: Reviews of Geophysics, v. 44, n. 1, RG1002, http://dx.doi.org/10.1029/2005RG000189

Tegner, C., 1997, Iron in plagioclase as a monitor of the differentiation of the Skaergaard intrusion: Contributions to Mineralogy and Petrology, v. 128, n. 1, p. 45–51, http://dx.doi.org/10.1007/s004100050292

Touret, J., ms, 1969, Le socle Précambrien de la Norvège méridionale: Nancy, France, Université de Nancy, Ph. D. thesis, 600 p.

Trindade, R. I. F., Raposo, M. I. B., Ernesto, M., and Siqueira, R., 1999, Magnetic susceptibility and partial anhysteretic remanence anisotropies in the magnetite-bearing granite pluton of Tourão, NE Brazil: Tectonophysics, v. 314, n. 4, p. 443–468, http://dx.doi.org/10.1016/S0040-1951(99)00220-6

Trindade, R. I. F., Bouchez, J. L., Bolle, O., Nédélec, A., Peschler, A., and Poitrasson, F., 2001, Secondary fabrics revealed by remanence anisotropy: methodological study and examples from plutonic rocks: Geophysical Journal International, v. 147, n. 2, p. 310–318, http://dx.doi.org/10.1046/j.0956-540x.2001.01529.x

Usui, Y., 2013, Paleointensity estimates from oceanic gabbros: Effects of hydrothermal alteration and cooling rate: Earth, Planets and Space, v. 65, n. 9, p. 985–996, http://dx.doi.org/10.5047/eps.2013.03.015

Usui, Y., Nakamura, N., and Yoshida, T., 2006, Magnetite microexsolutions in silicate and magmatic flow fabric of the Goyozan granitoid (NE Japan): Significance of partial remanence anisotropy: Journal of Geophysical Research: Solid Earth, v. 111, n. B11, http://dx.doi.org/10.1029/2005JB004183

Wenk, H. R., Chen, K., and Smith, R., 2011, Morphology and microstructure of magnetite and ilmenite inclusions in plagioclase from Adirondack anorthositic gneiss: American Mineralogist, v. 96, n. 8–9, p. 1316–1324, http://dx.doi.org/10.2138/am.2011.3760

Xu, W., Geissman, J. W., Van der Voo, R., and Peacor, D. R., 1997, Electron microscopy of iron oxides and implications for the origin of magnetizations and rock magnetic properties of Banded Series rocks of the Stillwater Complex, Montana: Journal of Geophysical Research: Solid Earth, v. 102, n. B6, p. 12139–12157, http://dx.doi.org/10.1029/97JB00303